Quantum measurements of sums

Juzar Thingna, Peter Talkner

Angaben zur Veröffentlichung / Publication details:

Thingna, Juzar, and Peter Talkner. 2020. "Quantum measurements of sums." *Physical Review A* 102 (1): 012213. https://doi.org/10.1103/physreva.102.012213.

Quantum measurements of sums

Juzar Thingna[1,*] and Peter Talkner[2,1,†]
[1]*Center for Theoretical Physics of Complex Systems, Institute for Basic Science (IBS), Daejeon 34126, Republic of Korea*
[2]*Institut für Physik, Universität Augsburg, Universitätsstrasse 1, D-86135 Augsburg, Germany*

(Received 29 February 2020; accepted 23 June 2020; published 13 July 2020)

A method is proposed that allows one to infer the sum of the values of an observable taken during contacts with a pointer state. Hereby, the state of the pointer is updated while contacted with the system and remains unchanged between contacts while the system evolves in time. After a prescribed number of such contacts, the position of the pointer is determined by means of a projective measurement. The outcome is specified in terms of a probability distribution function for unitary and Markovian dissipative dynamics and compared with the results of the same number of generalized Gaussian measurements of the considered observable. As a particular example, a qubit is considered with an observable contacting to the pointer that does not commute with the system Hamiltonian.

DOI: 10.1103/PhysRevA.102.012213

I. INTRODUCTION

Measurements play an important role in science, in general, and in quantum mechanics, in particular. While in classical systems measurements can, in principle, be performed with unlimited precision and without any influence on the measured object, for quantum systems often there are principle limits of the achievable precision and unavoidable, sometimes drastic backactions on the state of the measured object. The frequent repetition of the same measurement may either lead to the total freezing of the system's dynamics, known as the Zeno effect [1], or to a steady heating of the system [2,3], effects that are alien to classical systems. The emerging dissipative effects caused by so-called weak measurements of the continuous trajectory of an observable provide another instance of the unavoidable backaction of measurements in quantum systems [4–6].

Because the only way of gaining information about the state of a quantum system is by measuring, understanding the measurement process and its impact on the considered system is vital. From the point of view of a theoretician, projective measurements, wherein the system state collapses to the measured state [7], are most convenient. This idea of projective measurements leads to simple theoretical approaches, but lacks information about the measuring device and its properties as well as about possible deviations from the ideal picture. A more detailed scheme, originally also suggested by von Neumann [7,8], describes a measurement as an interaction of a system and a measurement apparatus, also called a pointer or a meter, to which the wished information about the system is transferred and finally read out. This approach is flexible in allowing the description of the measurement apparatus at a level as detailed as required for a specified study. In particular, it provides the means to adjust the precision of the measurement and, moreover, yields the according backaction on the system. The projective measurement of an observable is contained within this model in the limit of maximal precision. Moreover, in contrast to projective measurements, the von Neumann scheme is considerably more flexible in covering not only measurements of observables, given by Hermitian operators acting on the system Hilbert space, but is able to address more general questions, such as how to distinguish nonorthogonal states [9,10] or how to specify the difference of an observable at different times. In this way, the work performed by a an external stimulus on a system can be determined by a single measurement [11–13], in spite of the fact that work is not an observable [14]. Here the pointer is brought in contact with the system twice: the first time, immediately before the external stimulus sets in, and the second time, when the stimulus has ended. However, in contrast to the two-point measurement scheme of work [14], the result of the first contact is not immediately read out by means of a projective measurement, but rather stored and subtracted from the result of the final contact before the pointer is projectively read out.

Instead of differences, the sums of two or more values of a quantum observable may also be of interest such as in the theory of quantum walks [15]. Further, for a deeper understanding of reciprocating quantum engines [16,17], including how they behave and perform over many cycles, the sum of energies of the working substance repeatedly taken at the same instant within a cycle provides a promising diagnostic tool. However, when energies are determined by projective measurements, their backactions may have a considerable impact on the performance of the considered device [18–20]. Alternative tools to determine such sums are therefore of major importance.

In the present work, we demonstrate how the von Neumann scheme can be adapted to determine sums with high precision and, at the same time, as little backaction as possible. For this purpose, the values of an observable to be summed are transferred by repeated *contacts* to a pointer such as in the von Neumann scheme, however, without a readout of the pointer

*jythingna@ibs.re.kr
†peter.talkner@physik.uni-augsburg.de

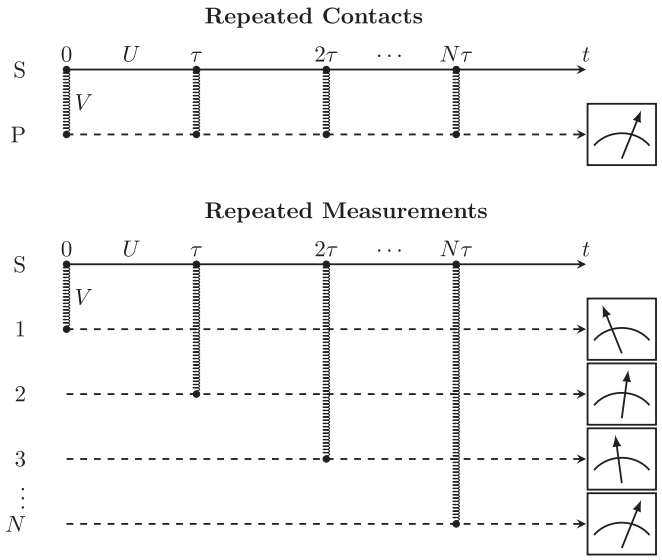

FIG. 1. Schematic illustration of the repeated contact and repeated measurement schemes. The solid lines represent the system evolution, whereas the dashed lines correspond to the pointer evolution. The system is periodically connected with the pointer at intervals of duration τ. The repeated contact scheme is less invasive as compared to the repeated measurements. The latter provides information about the full "trajectory" of measured values, while the former only allows one to infer about their sum.

following each contact. Instead, the state of the pointer is only determined after the required number of contacts has been performed. We develop the theory for the sum of an arbitrary observable of a general system taken at equally distant time points. The pointer is assumed to initially be prepared in a Gaussian state and its free dynamics to be trivial, such that its state is only altered by the contacts with the system. We compare the proposed repeated contacts approach to the repeated measurements case, where after each contact the measuring device is read out (see illustration in Fig. 1) for the same number N of contacts.

II. A SINGLE GENERALIZED MEASUREMENT

Following von Neumann's approach [7,8], we consider a quantum measuring device called a "pointer" that comes in contact with the system for a short time τ_p with strength g. The contact time is extremely short as compared to the timescale of system dynamics, such that the system does not evolve during the contact. Thus, whenever the pointer connects to the system, the density matrix $\rho_{\rm tot}$ of the combined system pointer immediately before the contact is modified to the postcontact state $\tilde{\rho}_{\rm tot}$ according to

$$\tilde{\rho}_{\rm tot} = V \rho_{\rm tot} V^\dagger, \tag{1}$$

where the unitary time evolution operator V, determined by the action of the system-pointer interaction Hamiltonian $H_{SP} = gMP$, is given by

$$V = e^{-i\kappa MP/\hbar}. \tag{2}$$

Here, the system operator M represents the observable to be measured and P is the momentum operator which is conjugate to the pointer position operator Q; finally, $\kappa = g\tau_p$ is an effective measure of the interaction strength. As an operator that is exponential in the pointer momentum operator P, V shifts the pointer position by an amount depending on the state of the system. If immediately after the system pointer contact a projective measurement of the pointer state with respect to the position x is performed, the non-normalized density matrix of the system follows by the action of the operation ϕ_x^1 [21–23], which is given by

$$\begin{aligned}\phi_x^1(\varrho) &= (x|\tilde{\rho}_{\rm tot}|x) \\ &= \sum_{m,m'} \mathcal{P}_m \varrho \mathcal{P}_{m'} \sigma(x - \kappa\mu_m, x - \kappa\mu_{m'}),\end{aligned} \tag{3}$$

where we assumed that the density matrix of the total system $\rho_{\rm tot}$ factorizes in a direct product of the density matrix of the system S, ϱ, and that of the pointer, σ. Here, $|x)$ is the eigenstate of the pointer position operator belonging to the eigenvalue x, and $e^{-iaP/\hbar}|x) = |x + a)$. Further, $\mathcal{P}_m$ is the projection operator of the system observable M onto the subspace belonging to the eigenvalue μ_m, and the position matrix elements of the pointer density matrix are denoted by

$$\sigma(x, y) = (x|\sigma|y). \tag{4}$$

The probability density function (PDF) $P_1(x)$ with which the pointer position x is observed is determined by the trace of the operation acting on the system density matrix, yielding

$$\begin{aligned}P_1(x) &= \mathrm{Tr}\, \phi_x^1(\varrho) \\ &= \sum_m p_m \sigma(x - \kappa\mu_m, x - \kappa\mu_m),\end{aligned} \tag{5}$$

where

$$p_m = \mathrm{Tr}\, \mathcal{P}_m \varrho \tag{6}$$

represents the probability to find a system with density matrix ϱ in the subspace belonging to the eigenvalue μ_m. For a pure Gaussian pointer state with vanishing mean values of the position and the momentum and the variance $\langle Q^2\rangle$, the density matrix takes the form

$$\sigma(x, y) = \frac{1}{\sqrt{2\pi\langle Q^2\rangle}} e^{-(x^2+y^2)/(4\langle Q^2\rangle)}. \tag{7}$$

Then, the PDF $P_1(x)$ becomes a mixture of Gaussians $g_{\langle Q^2\rangle}(x - \kappa\mu_n)$ with weights p_m, where $g_v(x) = (2\pi v)^{-1/2} \exp\{-x^2/(2v)\}$ denotes a Gaussian PDF with vanishing mean value and variance v. By rescaling the pointer variable according to $x = \kappa\,\mathsf{x}$, the maxima of the accordingly transformed PDF $P_1(\mathsf{x})$ are shifted towards the eigenvalues μ_m. The resulting scaled PDF hence becomes

$$P_1(\mathsf{x}) = \sum_m p_m\, g_{\sigma_{\mathsf{x}}^2}(\mathsf{x} - \mu_m). \tag{8}$$

In the mixture (8), those maxima survive whose weights are sufficiently large and for which the rescaled variance $\sigma_{\mathsf{x}}^2 = \langle Q^2\rangle/\kappa^2$ is sufficiently smaller than the squared smallest distance between the eigenvalues.

III. MULTIPLE CONTACTS

Rather than considering the statistics of the outcomes of a single measurement of some observable M, we are asking for the statistics of the sum of N values of the observable M that are assumed at subsequent times. The registration of the observable can be realized in different ways, which, in general, lead to different results. A straightforward procedure is to repeat the above-described generalized measurement N times always after the time τ has elapsed, as sketched in the lower panel of Fig. 1. We shall come back to this approach later. First, we follow the strategy illustrated in the upper panel of Fig. 1. This approach consists in N repetitions of contacts acting via the unitary operator V on the composed system, each followed by a unitary time evolution U of the system alone during a time τ while the pointer remains unaffected. The time evolution of the system from a contact to the next one is governed by the Hamiltonian H_S and hence given by

$$U = e^{-iH_S\tau/\hbar}. \tag{9}$$

The action of N combined contacts and time evolutions on the total, initially factorizing, density matrix is then given by

$$\rho_{\rm tot}(N\tau) = (UV)^N \varrho \otimes \sigma (V^\dagger U^\dagger)^N. \tag{10}$$

In analogy to the case of a single measurement, after the completion of the N contact protocol, one may read out the pointer state by a projective measurement. The non-normalized reduced density matrix conditioned on the measured result x is determined by the operation ϕ^N_{x}, which acts as

$$\begin{aligned}\phi^N_{\mathsf{x}}(\varrho) &= (\mathsf{x}|\rho_{\rm tot}(N\tau)|\mathsf{x}) \\ &= \sum_{\vec m,\vec m'} \rho_{\vec m,\vec m'} \sigma(\mathsf{x} - S_{\vec m}, \mathsf{x} - S_{\vec m'}),\end{aligned} \tag{11}$$

where $\vec m = (m_1, m_2, \ldots, m_N)$ and

$$\begin{aligned}\rho_{\vec m,\vec m'} &= U^N \mathcal{P}_{m_N}((N-1)\tau)\ldots\mathcal{P}_{m_2}(\tau)\mathcal{P}_{m_1}\varrho \\ &\times \mathcal{P}_{m'_1}\mathcal{P}_{m'_2}(\tau)\ldots\mathcal{P}_{m'_N}((N-1)\tau)U^{\dagger N}.\end{aligned} \tag{12}$$

Here, $\mathcal{P}_m(k\tau) = U^{k\dagger}\mathcal{P}_m U^k$ denotes a time-evolved projection operator. For a Gaussian pointer state as defined in Eq. (7), the position matrix element can be expressed as

$$\begin{aligned}\sigma(\mathsf{x} - S_{\vec m}, \mathsf{x} - S_{\vec m'}) &= g_{\sigma^2_{\mathsf{x}}}(\mathsf{x} - (S_{\vec m} + S_{\vec m'})/2) \\ &\times e^{-(S_{\vec m} - S_{\vec m'})^2/(8\sigma^2_{\mathsf{x}})}.\end{aligned} \tag{13}$$

The shift of the Gaussian is determined by sums of those N eigenvalues that are labeled by $\vec m$ and $\vec m'$, and hence reading

$$S_{\vec m} = \sum_{k=1}^{N} \mu_{m_k}, \tag{14}$$

and accordingly for the primed sequence $\vec m'$.

As in Eq. (5), the PDF $P_N(\mathsf{x})$ of finding the pointer at x after N contacts with the system is given by the trace over the non-normalized density matrix (11), and thus becomes

$$\begin{aligned}P_N(\mathsf{x}) = \sum_{\vec m,\vec m'} D^{\vec m,\vec m'}_{\varrho}\, g_{\sigma^2_{\mathsf{x}}}(\mathsf{x} - (S_{\vec m} + S_{\vec m'})/2) \\ \times e^{-(S_{\vec m} - S_{\vec m'})^2/(8\sigma^2_{\mathsf{x}})},\end{aligned} \tag{15}$$

with the coefficients $D^{\vec m,\vec m'}_{\varrho}$ reading

$$\begin{aligned}D^{\vec m,\vec m'}_{\varrho} &= {\rm Tr}\,\rho_{\vec m,\vec m'} \\ &= \delta_{m_N,m'_N}\,{\rm Tr}\,\mathcal{P}_{m'_1}\mathcal{P}_{m'_2}(\tau)\ldots\mathcal{P}_{m'_{N-1}}((N-2)\tau) \\ &\times \mathcal{P}_{m_N}((N-1)\tau)\ldots\mathcal{P}_{m_2}(\tau)\mathcal{P}_{m_1}\varrho.\end{aligned} \tag{16}$$

These coefficients constitute the elements of a non-negative definite tensor of rank N^2 guaranteeing the positivity of the PDF $P_N(\mathsf{x})$ in spite of some of them being complex quantities. In view of the result of N measurements discussed in the next section, we emphasize that the various Gaussian contributions to $P_N(\mathsf{x})$ all have the same variance $\sigma^2_{\mathsf{x}} = \langle Q^2\rangle/\kappa^2$, resulting from the variance of the initial pointer state and the measurement strength parameter κ. In particular, the width of these contributions is independent of the number of measurements. For a sufficiently narrow width, those contributions to the sum on the right-hand side of Eq. (15) stemming from vectors $\vec m$ and $\vec m'$ that lead to different sums $S_{\vec m}$ and $S_{\vec m'}$ are exponentially suppressed. Hence, if the inequality

$$8\sigma^2_{\mathsf{x}} \ll \min_{\substack{\vec m,\vec m' \\ S_{\vec m}\neq S_{\vec m'}}} (S_{\vec m} - S_{\vec m'})^2 = \min_{\substack{m,m', \\ m\neq m'}} (\mu_m - \mu_{m'})^2 \tag{17}$$

is satisfied, then the N contact strategy yields the statistics of the sums of eigenvalues of an observable M read out at equal intervals of length τ. In this case, one obtains, as the PDF of the sums, the following expression:

$$\begin{aligned}P_N(\mathsf{x}) &\approx \sum_{\substack{\vec m,\vec m' \\ S_{\vec m} = S_{\vec m'}}} D^{\vec m,\vec m'}_{\varrho}\, g_{\sigma^2_{\mathsf{x}}}(\mathsf{x} - \mathsf{S}_{\vec m}) \\ &= \sum_S w(S) g_{\sigma^2_{\mathsf{x}}}(\mathsf{x} - \mathsf{S}).\end{aligned} \tag{18}$$

Then the peaks of the PDF $P_N(\mathsf{x})$ are isolated, lying at the possible values S of the sums of N eigenvalues of the considered observable. The weights $w(S)$ are determined by the sums of the coefficient $D^{\vec m,\vec m'}_{\varrho}$ restricted to those trajectories $\vec m$ and $\vec m'$ yielding the same value S for the sum of the corresponding eigenvalues, and hence reading

$$w(S) = \sum_{\substack{\vec m,\vec m' \\ S_{\vec m} = S_{\vec m'} = S}} D^{\vec m,\vec m'}_{\varrho}. \tag{19}$$

In the special case in which the system Hamiltonian H_S and the observable M commute, the projection operators $\mathcal{P}_m$ are constants of motion, $\mathcal{P}_m(t) = \mathcal{P}_m$, and the coefficients $D^{\vec m,\vec m'}_{\varrho}$ simplify to read

$$D^{\vec m,\vec m'}_{\varrho} = \prod_{k=1}^{N-1} \delta_{m_k,m_{k+1}}\delta_{m_k,m'_k}, \tag{20}$$

yielding, for the N-contact PDF,

$$P_N(\mathsf{x}) = \sum_m p_m\, g_{\sigma^2_{\mathsf{x}}}(\mathsf{x} - N\mu_m), \tag{21}$$

with p_m defined in Eq. (6). This multiple-contact PDF resembles the single-measurement PDF (8) with the difference that all eigenvalues are multiplied by the number of contacts. The multiple-contact PDF is thus accordingly spread.

IV. MULTIPLE MEASUREMENTS

In order to perform N measurements of the same observable M at equally spaced times $n\tau, n = 0, 1, \ldots, (N-1)$, one may use the same number of equally prepared pointers, which are initially uncorrelated with each other as well as with the system. They are subsequently brought in contact with the system and, after the contact, read out by a projective measurement. Consequently, the non-normalized density matrix of the system conditioned on the sequence of measurements $\vec{\mathsf{x}} \equiv (\mathsf{x}_1, \mathsf{x}_2, \ldots, \mathsf{x}_N)$ takes the form

$$\begin{aligned} {}^m\phi_{\vec{\mathsf{x}}}(\varrho) &= \phi^1_{\mathsf{x}_N}\left[U\phi^1_{\mathsf{x}_{N-1}}\left(\ldots U\phi^1_{\mathsf{x}_1}(\varrho)U^\dagger\right)\ldots U^\dagger\right] \\ &= \sum_{\vec{m},\vec{m}'} \rho_{\vec{m},\vec{m}'} \prod_{k=1}^{N} g_{\sigma^2_{\mathsf{x}}}(\mathsf{x}_k - (\mu_{m_k} + \mu_{m'_k})/2) \\ &\quad \times e^{-(\mu_{m_k}-\mu_{m'_k})^2/(8\sigma^2_{\mathsf{x}})}. \end{aligned} \tag{22}$$

The PDF ${}^mP_N(\vec{\mathsf{x}})$ to find the sequence $\vec{\mathsf{x}}$ of the measurement is thus given by

$$\begin{aligned} {}^mP_N(\vec{\mathsf{x}}) &= \mathrm{Tr}\,{}^m\phi^N_{\vec{\mathsf{x}}}(\rho) \\ &= \sum_{\vec{m},\vec{m}'} D^{\vec{m},\vec{m}'}_{\varrho} \prod_{k=1}^{N} g_{\sigma^2_{\mathsf{x}}}(\mathsf{x}_k - (\mu_{m_k} + \mu_{m'_k})/2) \\ &\quad \times e^{-(\mu_{m_k}-\mu_{m'_k})^2/(8\sigma^2_{\mathsf{x}})}. \end{aligned} \tag{23}$$

Hence, the PDF ${}^mP_N(\mathsf{x})$ to find the value x for the sum of the individual measurement results becomes

$$\begin{aligned} {}^mP_N(\mathsf{x}) &= \int d^N\mathsf{x}\, \delta\left(\mathsf{x} - \sum_{k=1}^{N}\mathsf{x}_k\right) {}^mP_N(\vec{\mathsf{x}}) \\ &= \sum_{\vec{m},\vec{m}'} D^{\vec{m},\vec{m}'}_{\varrho}\, g_{N\sigma^2_{\mathsf{x}}}(\mathsf{x} - (S_{\vec{m}} + S_{\vec{m}'})/2) \\ &\quad \times \prod_{k=1}^{N} e^{-(\mu_{m_k}-\mu_{m'_k})^2/(8\sigma^2_{\mathsf{x}})}. \end{aligned} \tag{24}$$

As for the N-contact PDF (15), the N-measurement PDF of the sum is a linear combination of Gaussians with centers at the same positions $(S_{\vec{m}} + S_{\vec{m}'})/2$, but with the N-fold variances. Consequently, the N-contact PDF will, in general, have a much more detailed structure than the N-measurement PDF.

For a sufficiently small variance σ^2_{x}, the last product term in Eq. (24) suppresses all terms with $m_k \neq m'_k$. Therefore, only the diagonal part of the tensor $D^{\vec{m},\vec{m}'}_{\varrho}$ contributes. For any observable having a nondegenerate spectrum, it can be further simplified to read

$$D^{\vec{m},\vec{m}}_{\varrho} = \prod_{k=1}^{N-1} T(m_{k+1}|m_k)p_{m_1}, \tag{25}$$

where

$$T(m|n) = |\langle m|U|n\rangle|^2 \tag{26}$$

denotes the transition probabilities between eigenstates $|n\rangle$ and $|m\rangle$ of the observable M governed by the unitary dynamics U. These probabilities form a bistochastic transition matrix of a Markovian chain [24], with the number of measurements specifying the chain length. The coefficients $D^{\vec{m},\vec{m}}_{\varrho}$ are determined by the probability with which the sequence $\vec{m}$ starting at m_1 with probability p_1 occurs for this Markovian chain, where the number of states that can be taken at each step equals the dimension d_H of the Hilbert space of the system. For a large number of measurements, such a Markovian chain typically approaches a stationary regime in which the probability $1/d_H$ is assigned to all eigenvalues of the observable M. Hence the memory is lost of where the chain has started. Therefore, those vectors $\vec{m}$ with a uniform distribution of elements m_k acquire the highest probability for large N. One may expect that the average and the variance of the sums of N eigenvalues asymptotically both grow in proportion to N as in a normal random walk [25]. In exceptional cases, the Markovian chain may cause strictly periodic trajectories, which consequently also result in an asymptotically periodic variation of the variance of the eigenvalue sum.

Another exceptional case occurs when the transition matrix agrees with the identity, such as for observables commuting with the system Hamiltonian. Then, one obtains, with $T(m|n) = \delta_{m,n}$, the expression

$${}^mP_N(\mathsf{x}) = \sum_m p_m\, g_{N\sigma^2_{\mathsf{x}}}(\mathsf{x} - N\mu_m), \tag{27}$$

which leads, as for the corresponding N-contact protocol, to a mixture of Gaussians at the positions of the N-fold eigenvalues, however with substantially enlarged variances. In both cases, the variance of the eigenvalue sum grows as N^2.

V. DISSIPATIVE DYNAMICS

In the previous sections, the dynamics of the system between two consecutive contacts was considered to be governed by the unitary operator U. In most systems of practical interest, ensuring perfectly unitary dynamics is highly nontrivial and can only be achieved during a limited time span. In general, the implementation of the influence of an environment on the dynamics of a system, in general, poses a difficult problem. Here we assume weak coupling between the considered system and its environment, resulting in a Markovian dynamics of the system described by a Lindblad master equation [26]. This dynamics maps the density matrix from an instant after a contact with the pointer to a new state at a time τ later by means of a linear, completely positive and trace-preserving propagator $\mathcal{G}$. Hence, the initially factorizing density matrix of the total system after subsequent N contacts and Markovian propagation of the system becomes

$${}_d\rho_{\mathrm{tot}}(N\tau) = (\mathcal{G}\mathcal{V})^N(\varrho \otimes \sigma), \tag{28}$$

where $\mathcal{V}$ describes the action of a contact on the total density matrix, which is given by

$$\mathcal{V}(\rho_{\mathrm{tot}}) = V\rho_{\mathrm{tot}}V^\dagger, \tag{29}$$

with the unitary contact operator V defined in Eq. (2). As the result of a projective measurement of the pointer position after N contacts, one obtains, as the non-normalized density matrix conditioned on the measurement result x, an expression of the same structure as for a unitary dynamics, given by Eq. (11),

reading, for an initially Gaussian pointer state,

$$ {}_d\phi_x^N(\varrho) = \sum_{\vec{m},\vec{m}'} {}_d\rho_{\vec{m},\vec{m}'}\, g_{\sigma_x^2}(\mathsf{x} - (S_{\vec{m}} + S_{\vec{m}'})/2) \times e^{-(S_{\vec{m}} - S_{\vec{m}'})^2/(8\sigma_x^2)}, \tag{30} $$

where the system operators ${}_d\rho_{\vec{m},\vec{m}'}$ in the presence of a Markovian dissipative dynamics are defined as

$$ {}_d\rho^{\vec{m},\vec{m}'} = \mathcal{G}\{\mathcal{P}_{m_N}\mathcal{G}[\mathcal{P}_{m_{N-1}}\mathcal{G}(\ldots\mathcal{P}_{m_2}\mathcal{G}(\mathcal{P}_{m_1}\varrho\mathcal{P}_{m_1'}) \times \mathcal{P}_{m_2'}\ldots)\mathcal{P}_{m_{N-1}'}]\mathcal{P}_{m_N'}\}. \tag{31} $$

The probability ${}_dP_N(\mathsf{x})$ to find the result x again results from the trace of the non-normalized density matrix and hence becomes

$$ {}_dP_N(\mathsf{x}) = \sum_{\vec{m},\vec{m}'} {}_dD_\varrho^{\vec{m},\vec{m}'}\, g_{\sigma_x^2}(\mathsf{x} - (S_{\vec{m}} + S_{\vec{m}'})/2) \times e^{-(S_{\vec{m}} - S_{\vec{m}'})^2/(8\sigma_x^2)}. \tag{32} $$

It only differs from the above unitary result (15) through the form of the coefficient matrix, which is given by

$$ \begin{aligned} {}_dD_\varrho^{\vec{m},\vec{m}'} &= \mathrm{Tr}\,{}_d\rho_{\vec{m},\vec{m}'} \\ &= \delta_{m_N,m_N'}\mathrm{Tr}\,\mathcal{P}_{m_N}\mathcal{G}[\mathcal{P}_{m_{N-1}}\mathcal{G}(\ldots\mathcal{P}_{m_2} \\ &\quad\times\mathcal{G}(\mathcal{P}_{m_1}\varrho\mathcal{P}_{m_1'})\mathcal{P}_{m_2'}\ldots)\mathcal{P}_{m_{N-1}'}] \\ &= \delta_{m_N,m_N'}\mathrm{Tr}\,\mathcal{P}_{m_1'}\mathcal{G}^*(\mathcal{P}_{m_2'}\ldots\mathcal{G}^*(\mathcal{P}_{m_N}) \\ &\quad\ldots\mathcal{P}_{m_2})\mathcal{P}_{m_1}\varrho, \end{aligned} \tag{33} $$

with $\mathcal{G}^*$ denoting the dual propagator satisfying $\mathrm{Tr}\,u\mathcal{G}(\chi) = \mathrm{Tr}\,\mathcal{G}^*(u)\chi$ for all bounded operators u and all trace-class operators χ [27]. The last line can be identified with a multitime correlation function $\langle\mathcal{P}_{m_1'}\mathcal{P}_{m_2'}(\tau)\ldots\mathcal{P}_{m_N}((N-1)\tau)\ldots\mathcal{P}_{m_2}(\tau)\mathcal{P}_{m_1}\rangle$, as given by the quantum regression hypothesis [28], in analogy to the expression (16) for unitary dynamics. The Gaussians which are weighted by the above coefficients are located at the same positions and all have the same width as for a unitary dynamics.

Assuming that the Markovian dynamics asymptotically approaches a uniquely defined stationary state ρ^{st}, the propagator acts as $\mathcal{G}(\chi) = \rho^{st}\mathrm{Tr}\,\chi$ on all trace-class operators χ, provided that the time τ between subsequent measurements is large enough. Under this condition, the coefficients ${}_dD_\varrho^{\vec{m},\vec{m}'}$ simplify considerably to read

$$ {}_dD_\varrho^{\vec{m},\vec{m}'} = \delta_{\vec{m},\vec{m}'}p_{\vec{m}}, \tag{34} $$

where $p_{\vec{m}} = p_{m_1}\prod_{k=2}^N p_{m_k}^{st}$ with $p_m = \mathrm{Tr}\,\mathcal{P}_m\varrho$ and $p_{m_k}^{st} = \mathrm{Tr}\,\mathcal{P}_{m_k}\rho^{st}$ denotes the probability of finding the sequence of N eigenvalues $\mu_{\vec{m}}$ whose first member is drawn from the initial distribution and all others are independently taken from the stationary distribution. Further, we use, as a shorthand, $\delta_{\vec{m},\vec{m}'} \equiv \prod_{k=1}^N \delta_{m_k,m_k'}$. Hence, the PDF ${}_dP_N(\mathsf{x})$ simplifies to read

$$ {}_dP_N^{st}(\mathsf{x}) = \sum_{\vec{m}} g_{\sigma_x^2}(\mathsf{x} - S_{\vec{m}})p_{\vec{m}}. \tag{35} $$

Using the characteristic function of a Gaussian random variable given by $\int dx\, e^{iux}g_{\sigma^2}(x-S) = e^{iuS}e^{-u^2\sigma^2/2}$, one obtains the following expression for the characteristic function $G(u) = \int d\mathsf{x}\,{}_dP_N(\mathsf{x})\,e^{iu\mathsf{x}}$:

$$ G(u) = e^{-u^2\sigma_x^2}\mathrm{Tr}\,e^{iuM}\varrho\,(\mathrm{Tr}\,e^{iuM}\rho^{st})^{N-1}. \tag{36} $$

This expression, which is a product of the N characteristic functions of the observable M in the initial and subsequent stationary states, and of the characteristic function of the pointer position in its initial state, reflects the statistical independence of the individual contributions to the total outcome. Accordingly, the mean value ${}_d\langle\mathsf{x}\rangle = \int d\mathsf{x}\,{}_dP_N(\mathsf{x})\,\mathsf{x}$ and the variance ${}_d\Sigma_\mathsf{x}^2 = \int d\mathsf{x}\,{}_dP_N(\mathsf{x})\,(\mathsf{x} - {}_d\langle\mathsf{x}\rangle)^2$ result as

$$ {}_d\langle\mathsf{x}\rangle = \langle M\rangle_0 + (N-1)\langle M\rangle_{st}, \tag{37} $$

$$ {}_d\Sigma_\mathsf{x}^2 = \sigma_\mathsf{x}^2 + \langle(M - \langle M\rangle_0)^2\rangle_0 + (N-1)\langle\big(M - \langle M\rangle_{st}\big)^2\rangle_{st}, \tag{38} $$

with $\langle M\rangle_0 = \mathrm{Tr}M\varrho$ and $\langle M\rangle_{st} = \mathrm{Tr}M\rho^{st}$. For large values of contact numbers, the first moment as well as all cumulants grow proportionally to N. Hence, x behaves as a function of N as a random walk. In particular, the contribution x/N per step acquires asymptotically a Gaussian distribution. This will also remain true as an asymptotic result for large N if the time τ between two measurements is not large enough to lead to a complete approach to the stationary state. Due to its repeated action, any dissipative dynamics leading to a uniquely defined stationary state will generate a Gaussian random walklike behavior after sufficiently many contacts.

Finally, we note that a protocol with N measurements, as discussed in Sec. IV, in the presence of dissipation leads, for the sum of measurements, to an analogous expression as given in Eq. (24) with coefficients $D_\varrho^{\vec{m},\vec{m}'}$ replaced by ${}_dD_\varrho^{\vec{m},\vec{m}'}$. The main difference to the N-contact result (32) is the broadening of the individual Gaussian contributions.

VI. COMPARING THE IMPACT OF CONTACTS AND MEASUREMENTS

In order to quantify the average impact of repeated contacts on the state of the system, we determine the reduced density matrices ρ_k and ${}^m\rho_k$ of the system immediately after the kth contact and the kth measurement, respectively, and compare them with each other as well as with the density matrix $\rho(k\tau)$ which has evolved in the same time $k\tau$ in the absence of any contacts or measurements. The density matrix of the system after k contacts is obtained by performing the partial trace over the pointer state of the total density matrix, $\rho_{\mathrm{tot}}(k\tau) = \mathcal{V}(\mathcal{G}\mathcal{V})^{k-1}(\varrho\otimes\sigma)$, where $\mathcal{V}(\rho) = V\rho V^\dagger$. As above, $\mathcal{G}$ denotes the propagator of the Markovian dynamics between two contacts. In the case of unitary dynamics, it acts as $\mathcal{G}(\rho) = U\rho U^\dagger$; see, also, Eq. (10). Likewise, the reduced density matrix after k nonselective measurements is obtained as the k-fold trace over the pointers of the total density matrix, ${}^m\rho_{\mathrm{tot}}(k\tau) = \mathcal{V}_k[\mathcal{G}\mathcal{V}_{k-1}(\ldots\mathcal{G}\mathcal{V}_1(\rho\otimes\sigma_1)\ldots\otimes\sigma_{k-1})\otimes\sigma_k]$, where an index at the maps $\mathcal{V}$ indicates on which of the identical pointer state copies σ it acts. For a pointer initially staying in a Gaussian state, the partial pointer state trace can be performed to yield, for the reduced density

matrix after k contacts,

$$\rho_k = \sum_{{}^k\vec{m},{}^k\vec{m}'} R^{{}^k\vec{m},{}^k\vec{m}'} e^{-[\sum_{j=1}^k(\mu_{m_j}-\mu_{m'_j})]^2/(8\sigma_{\mathsf{x}}^2)}, \tag{39}$$

where ${}^k\vec{m}$ denotes a vector whose number of components is k and whose components are taken from the set indexing the eigenvalues of the tested observable M. Further, $R^{{}^k\vec{m},{}^k\vec{m}'}$ is a trace-class operator of the system indexed by a double series of left- and right-hand shifts of the pointer state. It is defined as

$$R^{{}^k\vec{m},{}^k\vec{m}'} = \mathcal{P}_{m_k}\mathcal{G}(\mathcal{P}_{m_{k-1}}\ldots\mathcal{G}(\mathcal{P}_{m_1}\varrho\mathcal{P}_{m'_1})\mathcal{P}_{m'_{k-1}})\mathcal{P}_{m'_k}. \tag{40}$$

In contrast, after k nonselective measurements, the reduced density matrix is given by

$$\rho_k^m = \sum_{{}^k\vec{m},{}^k\vec{m}'} R^{{}^k\vec{m},{}^k\vec{m}'} e^{-\sum_{j=1}^k(\mu_{m_j}-\mu_{m'_j})^2/(8\sigma_{\mathsf{x}}^2)}. \tag{41}$$

Both the k-contact and the k-measurement density matrices are linear combinations of the contact-specific operators $R^{{}^k\vec{m},{}^k\vec{m}'}$, however being weighted by different coefficients. In the limit of a very wide initial pointer state, $\sigma_{\mathsf{x}}^2 \to \infty$, these coefficients approach unity. With the completeness of the projection operators, $\sum_m \mathcal{P}_m = \mathbb{1}$, all sums can be performed and, in both cases, the backaction-free density matrix results equally for k contacts and k measurements, i.e.,

$$\begin{aligned}\lim_{\sigma_{\mathsf{x}}\to\infty}\rho_k &= \lim_{\sigma_{\mathsf{x}}\to\infty}\rho_k^m \\ &= \sum_{{}^k\vec{m},{}^k\vec{m}'} R^{{}^k\vec{m},{}^k\vec{m}'} = \mathcal{G}^{k-1}(\rho).\end{aligned} \tag{42}$$

In the other limit of precise measurements when the variance σ_{x}^2 is larger than zero but satisfies the inequality (17), the exponential factors on the right-hand side of Eq. (41) suppress all nondiagonal contributions after multiple measurements and one finds

$$\lim_{\sigma_{\mathsf{x}}\to 0}\rho_k^m = \sum_{{}^k\vec{m}} R^{{}^k\vec{m},{}^k\vec{m}}, \tag{43}$$

as for k nonselective projective measurements. In contrast, in the same limit for k contacts, only those nondiagonal elements of the reduced density matrix are suppressed that belong to pairs of sequences ${}^k\vec{m}$ and ${}^k\vec{m}'$ with different eigenvalue sums $S_{{}^k\vec{m}} \neq S_{{}^k\vec{m}'}$, thus yielding

$$\lim_{\sigma_{\mathsf{x}}\to 0}\rho_k = \sum_{\substack{{}^k\vec{m},{}^k\vec{m}' \\ S_{\vec{m}}=S_{\vec{m}'}}} R^{{}^k\vec{m},{}^k\vec{m}'}. \tag{44}$$

Therefore, in this limit, coherences with respect to the eigenbasis of the observable M are much less suppressed than in the measurement scheme.

Finally, we note that in the limit of large τ for dissipative dynamics, such that stationarity is reached, one obtains the same result for multiple contacts and multiple measurements, reading

$$\rho_k^{(m)} = \sum_{m_k,m'_k} \mathcal{P}_{m_k}\rho^{st}\mathcal{P}_{m'_k} e^{-(\mu_{m_k}-\mu_{m'_k})^2/8\sigma_{\mathsf{x}}^2}. \tag{45}$$

Note that this density matrix is independent of the number of contacts or measurements because the dynamics between contacts or measurements erases any memory on the prehistory. For the example discussed below, the deviations of the reduced density matrices after k contacts and k measurements from the unperturbed time-evolved density matrix are quantified by means of the respective trace distances.

VII. EXAMPLE: QUBIT

In order to illustrate the general theory outlined in the previous section, we consider a quantum qubit as the system of interest whose Hamiltonian reads

$$H = \hbar B\boldsymbol{\tau}_z, \tag{46}$$

with $\boldsymbol{\tau}_z$ being the z component of the Pauli spin-1/2 matrix and B being the strength of the Hamiltonian. We measure $\boldsymbol{\tau}_x$ for the qubit such that the operator $M = \boldsymbol{\tau}_x$. We first consider the case of unitary dynamics

A. Unitary dynamics

In spite of the fact that both the time evolution of the free qubit, given by $U = \cos\theta - i\boldsymbol{\tau}_z\sin\theta$, and the spectral representation of M with $\mu_1 = -1$, $\mathcal{P}_1 = (1-\boldsymbol{\tau}_x)/2$ and $\mu_2 = 1$, $\mathcal{P}_2 = (1+\boldsymbol{\tau}_x)/2$ are very simple, the exponential growth of the number of terms contributing to the PDF (15) characterizing the N-contact protocol renders its analytic presentation for more than $N = 2$ contacts basically impossible. Here, $\theta = B\tau$ specifies the duration of the unitary time evolution between two contacts in units of the inverse frequency of the qubit. For $N = 2$, one obtains, after some lengthy algebra, the expression

$$\begin{aligned}P_2(\mathsf{x}) = \frac{1}{\sqrt{2\pi\sigma_{\mathsf{x}}^2}}\Big[&\Big(p_1 e^{-\frac{(\mathsf{x}+2)^2}{2\sigma_{\mathsf{x}}^2}} + p_2 e^{-\frac{(\mathsf{x}-2)^2}{2\sigma_{\mathsf{x}}^2}}\Big)\cos^2\theta \\ &+ e^{-\frac{\mathsf{x}^2}{2\sigma_{\mathsf{x}}^2}}\sin^2\theta \\ &+ q\,e^{-\frac{1}{2\sigma_{\mathsf{x}}^2}}\Big(e^{-\frac{(\mathsf{x}+1)^2}{2\sigma_{\mathsf{x}}^2}} - e^{-\frac{(\mathsf{x}-1)^2}{2\sigma_{\mathsf{x}}^2}}\Big)\sin 2\theta\Big],\end{aligned} \tag{47}$$

where $p_i = \mathrm{Tr}\,\mathcal{P}_i\varrho$, as defined in Eq. (6), $q = \mathrm{Tr}\,\boldsymbol{\tau}_y\varrho/2$, and $w = \mathrm{Tr}\,\boldsymbol{\tau}_z\varrho/2$ is restricted by $w^2 + q^2 \leqslant p_1p_2$ because of the positivity of the initial density matrix ϱ. For sufficiently small variances, say $\sigma_{\mathsf{x}}^2 \lesssim 0.1$, one observes well-separated peaks at the positions $\mathsf{x} = 0, \pm 2$. At larger variances, the peaks merge into a broad distribution. The contributions at $\mathsf{x} = \pm 1$ are never visible as peaks. At small variances, their contribution is exponentially suppressed; at larger ones, they influence the form of the PDF as seen in Fig. 2. The peak heights are governed by the probabilities p_1 and p_2 with which the eigenstates of the measured operator $\boldsymbol{\tau}_x$ with corresponding eigenvalues $\mu_1 = -1$ and $\mu_2 = 1$, respectively, contribute to the initial density matrix ϱ. Since we choose the state with $\mu = -1$ to have a higher occupancy, the distribution is skewed to negative x, a property that is carried forward to large N, as seen in Fig. 3.

Another analytic result emerges for $\theta = n\pi$. In this case, the time-evolution operator U commutes with the observable M and hence yields, with Eq. (21), a bimodal PDF [Figs. 3(c) and 3(f); red solid lines],

$$P_N(\mathsf{x})|_{\theta=\pi} = \frac{1}{\sqrt{2\pi\sigma_{\mathsf{x}}^2}}\Big(p_1 e^{-\frac{(\mathsf{x}+N)^2}{2\sigma_{\mathsf{x}}^2}} + p_2 e^{-\frac{(\mathsf{x}-N)^2}{2\sigma_{\mathsf{x}}^2}}\Big). \tag{48}$$

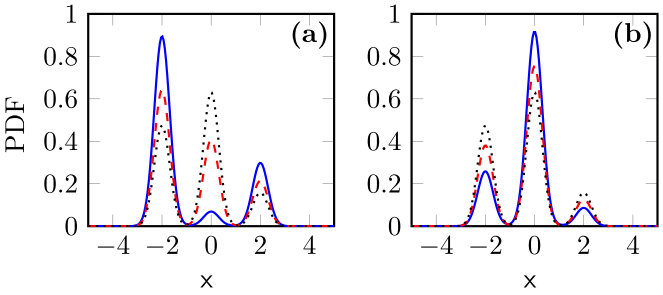

FIG. 2. The PDFs $P_2(\mathsf{x})$ (blue solid lines) for unitary dynamics and ${}_dP_2(\mathsf{x})$ for dissipative dynamics at different dissipation rates (red dashed and black dotted lines) given by Eqs. (47) and (51) characterizing unitary and dissipative dynamics. For unitary dynamics, the relative weights of the central peak at $\mathsf{x} = 0$ and the two side peaks $\mathsf{x} = \pm 2$ depend on the time between two contacts (a) $\theta = B\tau = 11.7\pi/4$ and (b) $\theta = 10.7\pi/4$. In the presence of dissipation $[\gamma = (\Gamma_1 + \Gamma_2)/B = 0.1]$, the height ratio of the side peaks stays constant, while they exchange weight with the central peak (red dashed lines). In the limit $r^d = \theta\gamma \to \infty$, the weights of the central peak equals the sum of the weights of the side peaks [black dotted curves in (a) and (b)]. For all cases, the initial density matrix is $\boldsymbol{\tau}_x = 0.5$, yielding $p_1 = \mathrm{Tr}\mathcal{P}_1\varrho = 0.75$; further, $q = \mathrm{Tr}\boldsymbol{\tau}_y\varrho/2 = 0.43$ and $w = \mathrm{Tr}\,\boldsymbol{\tau}_z\varrho/2 = 0$. The initial Gaussian state has variance $\sigma_\mathsf{x}^2 = 0.1$.

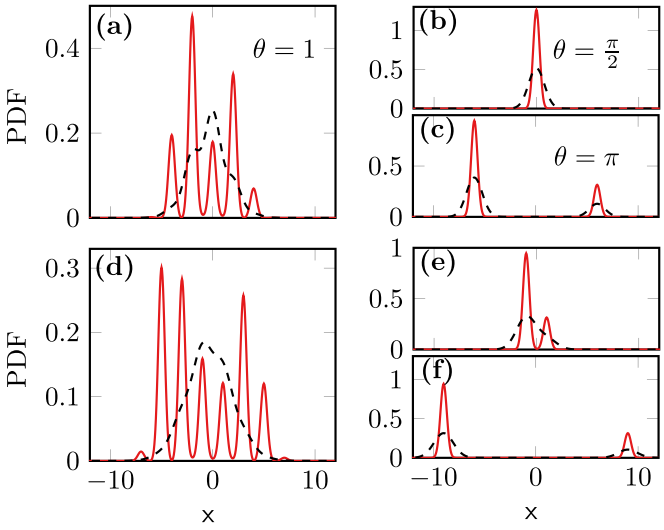

FIG. 3. The PDF $P_N(\mathsf{x})$ given by Eq. (15) of the pointer state after (a)–(c) $N = 6$ and (d)–(f) $N = 9$ contacts with a unitarily evolving qubit is displayed as a function of x (red solid lines) together with the corresponding PDFs ${}^mP_N(\mathsf{x})$ [Eq. (24)] characterizing multiple measurements (black dashed lines). The time between two contacts, as well as between two measurements, is (a),(d) $\theta = 1$, (b),(e) $\theta = \pi/2$, and (c),(f) $\theta = \pi$. For all cases, the initial density matrix is determined by $\langle\boldsymbol{\tau}_x\rangle = 0.5$, $\langle\boldsymbol{\tau}_y\rangle = 0$, and $\langle\boldsymbol{\tau}_z\rangle = 0.78$. The initial Gaussian pointer state has variance $\sigma_\mathsf{x}^2 = 0.1$, leading, for the contact scheme at the generic value $\theta = 1$, to well-separated lines centered at all but the two extreme positions of possible sums of the two eigenvalues ($\mu = \pm 1$). The extreme positions have a too small weight to be visible. For the exceptional value $\theta = \pi/2$ and $N = 6$, there is only a single line centered at $\mathsf{x} = 0$ and two lines for $N = 9$ at the positions of the eigenvalues, $\mathsf{x} = \pm 1$. For the other exceptional period $\theta = \pi$, two lines are located at $\mathsf{x} = \pm N$. The width of the individual lines is always determined by σ_x for repeated contacts. For repeated measurements, the individual contributions merge to yield broad distributions. Only for $\theta = \pi$, the lines remain visible as they are separated by $2N$ and the width is proportional to $\sqrt{N}$.

For this limiting case, the average becomes $\langle\mathsf{x}\rangle = N(p_1 - p_2)$ and the variance $\Sigma_\mathsf{x}^2 = \langle\mathsf{x}^2\rangle - \langle\mathsf{x}\rangle^2 = \sigma_\mathsf{x}^2 + 2p_1N^2$. The repeated measurement case [Eq. (24); Figs. 3(c) and 3(f), black dashed lines] can also be analytically evaluated for $\theta = \pi$, resulting in a similar expression as above with $\sigma_\mathsf{x}^2 \to N^2\sigma_\mathsf{x}^2$.

In general, the PDF for a repeated contact $P_N(\mathsf{x})$ displays a complex behavior, as shown by the red solid lines in Figs. 3(a) and 3(d). As expected, performing repeated measurements significantly broadens the PDF and we lose all individual measurement-related information even for a small number of measurements [see Figs. 3(a) and 3(d)].

Yet another special case turns out to be $\theta = \pi/2$. Because the time evolution flips the projection operators $\mathcal{P}_m(n\pi/2) = \mathcal{P}_{(-1)^n m}$ for n odd, and leaves them unchanged for n even, a unimodal PDF, being centered at $\mathsf{x} = 0$, emerges for any even number of contacts [$N = 6$, see Fig. 3(b)], while it becomes bimodal with a higher weight at negative values of x (due to the initial ϱ with $p_1 > p_2$) for an odd number of contacts [$N = 9$, see Fig. 3(e)]. The behavior as a function of θ is captured in Fig. 4, displaying a perfect bimodal distribution occurring at $\theta = 0, \pi/2, \pi$. At all other values, intermediate peaks of the distribution are visible, but much weaker as compared to the dominant peak at negative x skewing the average to negative values of x.

We restrict the discussion of repeated measurements to cases with a sufficiently narrow initial pointer state variance σ_x^2. The PDF ${}^mP_N(\mathsf{x})$ characterizing the N measurement scheme then contains only diagonal coefficients $D_\varrho^{\vec{m},\vec{m}}$, which are determined by a transition matrix with the elements $T(1|1) = T(2|2) = \cos^2\theta$ and $T(1|2) = T(2|1) = \sin^2\theta$; see Eqs. (25) and (26). With an increasing number of N, the relatively narrow lying lines typically merge, resulting in a broad PDF with a most probable value at $\mathsf{x} \approx 0$. Accordingly, the variance grows proportional to N for all generic values of θ, such as $\theta = 1$; see the black dashed curves displayed in Figs. 3(a) and 3(d). The exceptional cases $\theta = n\pi, n = 0, 1, 2$ yield the identity for the transition matrix. According to Eq. (27), the PDF ${}^mP_N(\mathsf{x})$ displays two separate lines at $\pm N$, each of which has a width proportional to N [see Figs. 3(c) and 3(d), and Figs. 6(a) and 6(c)]. Consequently, the variance Σ_x^2 increases as N^2. On the other hand, the choice $\theta = \pi/2, 3\pi/2$ leads to a periodic Markov chain, which entails an alternatingly uni- and bimodal PDF for even and odd N, respectively. Then, the variance is also periodic [see, also, Figs. 6(a) and 6(c)].

B. Dissipative dynamics

Next, we discuss the case of dissipative dynamics, which is assumed to be governed by a Lindblad-type master equation [29] reading

$$\dot{\rho}(t) = -iB[\boldsymbol{\tau}_z, \rho(t)] + \Gamma_1([\boldsymbol{\tau}_-, \rho\boldsymbol{\tau}_+] + [\boldsymbol{\tau}_-\rho, \boldsymbol{\tau}_+]) + \Gamma_2([\boldsymbol{\tau}_+, \rho\boldsymbol{\tau}_-] + [\boldsymbol{\tau}_+\rho, \boldsymbol{\tau}_-]), \quad (49)$$

where $\Gamma_1 > \Gamma_2$. The operators $\boldsymbol{\tau}_z$, $\boldsymbol{\tau}_+ = (\boldsymbol{\tau}_x + i\boldsymbol{\tau}_y)/2$, $\boldsymbol{\tau}_- = (\boldsymbol{\tau}_x - i\boldsymbol{\tau}_y)/2$ and $\mathbb{1}$ form a complete set, which transforms

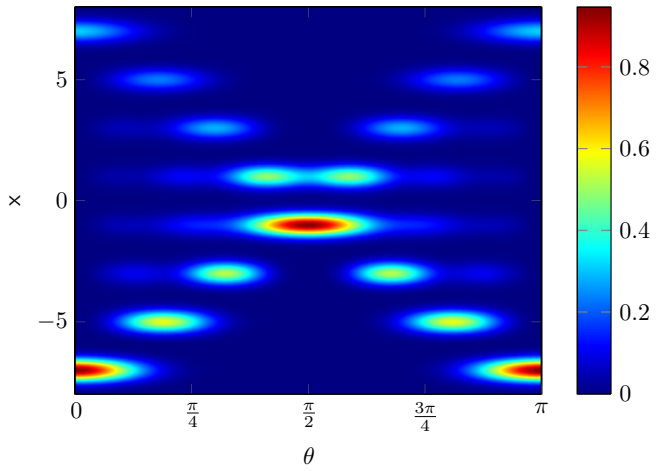

FIG. 4. A color-coded presentation of the PDF $P_7(\mathsf{x})$ as a function of the duration of the time θ and the pointer position x. For generic values of θ, the PDF exhibits local maxima at the possible values of the sums of seven eigenvalues ± 1 at $-7, -5, \ldots, 5, 7$. For particular times $\theta = 0, \pi$, the bimodal PDF (48) and, for $\pi/2$, a unimodal PDF with maximum at $\mathsf{x} = 0$ results. All distributions disclose a bias towards a negative value due to the chosen initial density matrix which was chosen as specified in Fig. 3.

under the dual propagator as

$$\mathcal{G}^*(\boldsymbol{\tau}_+) = e^{(2i-\gamma)\theta}\boldsymbol{\tau}_+, \quad \mathcal{G}^*(\boldsymbol{\tau}_-) = e^{-(2i+\gamma)\theta}\boldsymbol{\tau}_-,$$
$$\mathcal{G}^*(\boldsymbol{\tau}_z) = e^{-2\gamma\theta}\boldsymbol{\tau}_z + \frac{\Gamma_1-\Gamma_2}{\Gamma_1+\Gamma_2}(1-e^{-2\gamma\theta})\mathbb{1}, \quad \mathcal{G}^*(\mathbb{1}) = \mathbb{1}. \tag{50}$$

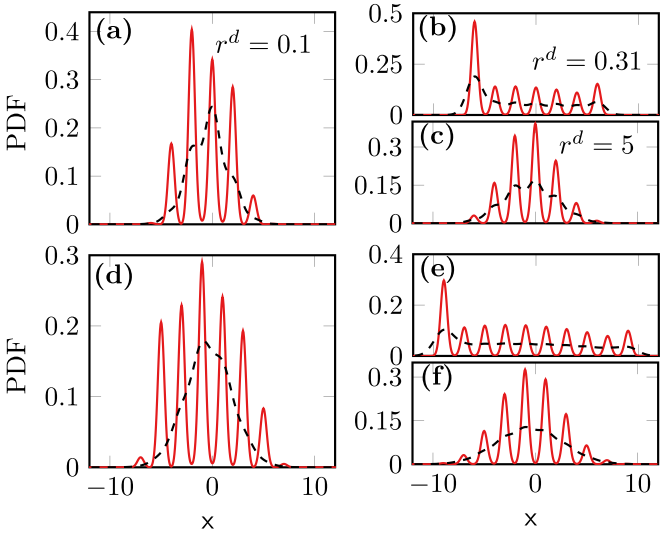

FIG. 5. The multiple contact PDF ${}_dP_N(\mathsf{x})$ [Eq. (32), red solid lines] and the repeated measurement PDF ${}^m_dP_N(\mathsf{x})$ (black dashed lines) are displayed as functions of the pointer position x for various dissipation ratios (a), (d) $r^d = \gamma\theta = 0.1$, (b), (e) $r^d = 0.31$, and (c), (f) $r^d = 5$. (a)–(c) $N = 6$ and (d)–(f) $N = 9$. The individual rates are chosen as $\Gamma_1/B = 7.5 \times 10^{-2}$ and $\Gamma_2/B = 2.5 \times 10^{-2}$. The initial density matrix of the qubit and the initial variance of the pointer are chosen as in Fig. 3.

Here, the dimensionless damping rate is defined as $\gamma = (\Gamma_1 + \Gamma_2)/B$. Similarly as in the unitary case, we can find the analytic form of the distribution when two measurements are made ($N = 2$),

$$\begin{aligned} {}_dP_2(\mathsf{x}) = \frac{1}{\sqrt{2\pi\sigma_\mathsf{x}^2}}\Big[&\Big(p_1 e^{-\frac{(\mathsf{x}+2)^2}{2\sigma_\mathsf{x}^2}} + p_2 e^{-\frac{(\mathsf{x}-2)^2}{2\sigma_\mathsf{x}^2}}\Big) f_c(\theta) \\ &+ e^{-\frac{\mathsf{x}^2}{2\sigma_\mathsf{x}^2}} f_s(\theta) \\ &+ q e^{-\frac{1}{2\sigma_\mathsf{x}^2}}\Big(e^{-\frac{(\mathsf{x}+1)^2}{2\sigma_\mathsf{x}^2}} - e^{-\frac{(\mathsf{x}-1)^2}{2\sigma_\mathsf{x}^2}}\Big) e^{-\gamma\theta}\sin 2\theta\Big], \end{aligned} \tag{51}$$

with

$$f_c(\theta) = (1 + e^{-\gamma\theta}\cos 2\theta)/2,$$
$$f_s(\theta) = (1 - e^{-\gamma\theta}\cos 2\theta)/2. \tag{52}$$

In the absence of dissipation, Eq. (51) maps exactly to Eq. (47). The presence of any finite dissipation exponentially reduces the influence of the Gaussian contributions at $\mathsf{x} = \pm 1$.

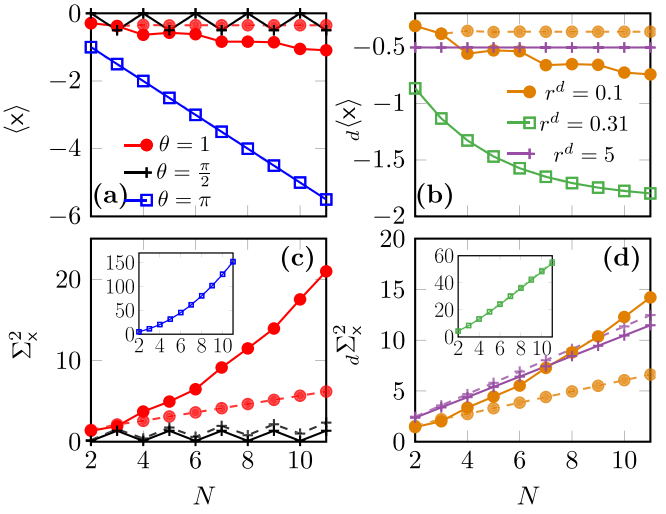

FIG. 6. (a), (b) The mean values $\langle \mathsf{x} \rangle$ and (c), (d) the variances Σ_x^2 of the pointer position as a function of the number of repeated contacts (solid lines) and the number of repeated measurements (dashed lines) for (a), (c) unitary and for (b), (d) dissipative dynamics. For unitary dynamics with the atypical duration $\theta = \pi/2$, the oscillation of the PDF between a bimodal and a unimodal form leads to an oscillatory behavior of the mean and an N-independent variance [black plus symbols in (a) and (c)] for repeated contacts. For repeated measurements, the mean follows the same oscillatory behavior with the variance of each Gaussian peak scaling with N, giving Σ_x^2 a weak dependence on N. For $\theta = \pi$, both the repeated contact and measurement schemes yield, with Eqs. (21) and (27), respectively, a linear increase of the absolute mean value $\langle \mathsf{x} \rangle$ and a quadratic increase of the variance Σ_x^2, as displayed in the inset of (c). For typical values of θ, the repeated contact scheme with unitary dynamics gives rise to a qualitatively similar, but less pronounced ballistic diffusion behavior. In contrast, repeated measurements lead to a saturation of the mean value and a linear growth of the variance, i.e., to normal diffusion of x. A transition to normal diffusion is also observed in the presence of dissipation. For the largest dissipation with $r^d = 5$, the mean value and the variance are in good agreement with Eqs. (37) and (38). Other parameters are chosen as in Fig. 3.

Further, it changes the relative weights of the peaks at $\mathsf{x} = \pm 2$ and $\mathsf{x} = 0$: The side peaks increase if $\cos 2\theta > 0$ [Fig. 2(a), blue solid line], while the central peak grows if $\cos 2\theta < 0$ [Fig. 2(b), blue solid line]. In the limit of large times $\theta \to \infty$, the asymptotic result following from Eq. (35) for $N = 2$ is approached (Fig. 2, black dotted lines). This is because the stationary density matrix resulting from the master equation (49) is diagonal with respect to the $\boldsymbol{\tau}_z$ eigenbasis such that both stationary probabilities $p^{st}_{1,2}$ have the same value of $1/2$, independent of the stationary expectation value, $\langle \boldsymbol{\tau}_z \rangle_{st} = (\Gamma_1 - \Gamma_2)/(\Gamma_1 + \Gamma_2)$.

For two larger values of N, some results are presented in Fig. 5. For the small dissipation parameter $r^d \equiv \gamma\theta = 0.1$, the system does not have enough time to thermalize between measurements and hence the PDFs displayed in Figs. 3(a) and 3(d) resemble those for unitary dynamics. At the intermediate value of $r^d = 0.31$, the additional two peaks at the maximal positions $\mathsf{x} = \pm N$ become visible with maximal weight at $-N$, while all other peaks are of approximately the same height; see Figs. 3(b) and 3(e). With a further increase of the dissipation parameter, the system between two measurements is driven into the stationary state, yielding the asymptotic result given by Eq. (35) for the PDF. It takes a further simplified form for any initial density matrix that commutes with $\boldsymbol{\tau}_z$ such that, with $p_{\vec{m}} = (1/2)^N$, the PDF assumes the form of a mixture of Gaussians with binomial weights. The centers of these Gaussians are located at the possible values taken by the sums of all combinations of eigenvalues. The binomial weights reflect the number of different combinations of N eigenvalues with the same sum. In this particular case, the PDF hence reads

$$ {}_dP^{st}_N(\mathsf{x}) = \left(\frac{1}{2}\right)^N \sum_{k=0}^{N} \binom{N}{k} g_{\sigma^2_{\mathsf{x}}}(\mathsf{x} - N + 2k). \tag{53}$$

In spite of the fact that the initial state has an off-diagonal matrix element with respect to the $\boldsymbol{\tau}_z$ basis, the agreement of the results displayed in Figs. 5(c) and 5(f) is very good.

A rough characterization of the N dependence of the statistics of x, specifying either the number of contacts or of measurements, both for the unitary and the dissipative case, is provided by the mean value and the variance, $\langle \mathsf{x} \rangle$ and Σ^2_{x}, as displayed for a few cases in Fig. 6. Typically, the mean value grows proportionally to the number of contacts as well as to the number of measurements, both for unitary and for dissipative dynamics, as illustrated by the upper two panels of Fig. 6. An exception from this rule occurs for $\theta = \pi/2$, displaying oscillations of the mean value for unitary dynamics in agreement with the above-described behavior of the underlying PDFs alternating as a function of N between the same unimodal and bimodal shapes.

The influence of dissipation suppresses correlations between the shifts of the pointer states at contacts that are separated by a sufficiently large dissipation ratio r^d, leading to a variance asymptotically growing proportionally to the number of contacts displaying the characteristic feature of normal diffusion. For the here-considered most simple qubit, and as we also expect for other so-called integrable quantum systems [30], the variance increases with N^2 as in the case of classical, ballistic diffusion. This observation, though, is based on our numerical results, which are restricted to a relatively low number of contacts. One might speculate that for unitary chaotic dynamics, the variance still grows superdiffusively, but governed by a power law with an exponent between one and two. The different behavior of unitary and dissipative dynamics for a qubit is illustrated in Figs. 6(c) and 6(d), respectively.

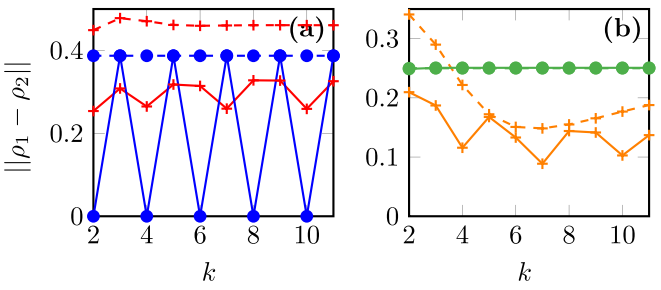

FIG. 7. The trace distances $||\rho_1 - \rho_2||$ according to Eq. (54) from a density matrix $\rho_2 \equiv \rho(k\theta)$ uninterruptedly evolved up to the time $k\theta$, either by (a) unitary or (b) dissipative dynamics, to the corresponding dynamical scheme ρ_1 with k repeated contacts (solid lines) or k measurements (dashed lines). In the case of unitary dynamics, the time between contacts or measurements is $\theta = 1$ (red plus symbols) and $\theta = \pi/2$ (blue closed circles). In the case of dissipative dynamics, results are displayed for the dissipation rates $r^d = 0.1$ (orange plus symbols) and $r^d = 5$ (green closed circles). Typically, the distance between the interrupted and uninterrupted scenario is smaller for repeated contacts than for repeated measurements, indicating a less severe backaction by the contacts compared to the measurements. Exceptions are found for unitary dynamics at $\theta = \pi/2$ with an odd number of interruptions and for the case of the large dissipation rate leading to an almost perfect approach to the stationary state of the qubit. The remaining parameters are chosen as in Fig. 3. The lines connecting the points at integer values of k are meant to guide the eye.

C. Trace distance

In Fig. 7, the trace distances between the density matrices of systems affected by a number of contacts or measurements and those freely propagating are compared as a function of the number of contacts. Here we use the trace distance between two density matrices ρ_α ($\alpha = 1, 2$), describing qubits having the expectation values $\langle \boldsymbol{\tau}_k \rangle^\alpha = \mathrm{Tr}\, \boldsymbol{\tau}_k \rho_\alpha$ ($k = x, y, z$), given by

$$ ||\rho_1 - \rho_2|| \equiv \mathrm{Tr}|\rho_1 - \rho_2| = \left[\sum_k (\langle \boldsymbol{\tau}_k \rangle^1 - \langle \boldsymbol{\tau}_k \rangle^2)^2 \right]^{1/2}. \tag{54}$$

It turns out that the trace distance is typically smaller for the less-invasive repeated contact scheme (solid lines) than for repeated measurements (dashed lines) in Fig. 7. In the case of repeated contacts with unitary dynamics in between with $\theta = \pi/2$ [blue solid lines with closed circles in Fig. 7(a)], the odd number of contacts and measurements results in the same trace distance because then one finds operators $R^{k\vec{m},k\vec{m}'} = \prod_{l=1}^{k} \delta_{m_l,m'_l} \mathcal{P}_{m_k} \rho \mathcal{P}_{m_k}$ yielding equal exponential weights in Eqs. (39) and (41). The other exception from the rule is for complete equilibration where the k contacts and k measure-

ments lead to the same density matrix; see Eq. (45) [green closed circles in Fig. 7(b)].

VIII. CONCLUSIONS

We investigated in some detail a particular strategy to gain information about the values of an observable taken at subsequent times with as little backaction on the system as possible. The primary information on the system is taken within intervals of time that are negligibly short; it is transferred to the state of a pointer where their subsequent contributions are accumulated. After each contact, the system is allowed to move freely, i.e., without being influenced by the pointer. The pointer itself is assumed to be idle until it is contacted again. The final readout of the pointer in terms of a projective measurement yields a value that coincides, within some error margin, with the sum of the observable at the instants of contacts. Other values, corresponding to the algebraic mean of two such sums, are exponentially suppressed as long as the mentioned error margin is narrow enough.

The resulting statistics of the final pointer state may be interpreted in terms of discrete quantum walks [15]. Here, the walker is realized by the pointer and the system performs as the coin deciding in which direction and how far the walker moves in a step. In the example of a qubit, the Hilbert space of the coin has dimension two, as frequently assumed in the theory of quantum walks but generalizations to coins living in arbitrarily large Hilbert spaces are straightforward. Discrete quantum walks performing a small number of steps on a lattice can be used as generalized measurements distinguishing nonorthogonal states [31–33].

In general, depending on the kind of dynamics of the system, the resulting random walk may vary from ballistic, i.e., with a variance growing proportionally to the square of the number of steps, to normal diffusion, with a linear growth of the variance. The latter behavior is found for dissipative dynamics of the system governed by a Markovian master equation. For the qubit, undergoing unitary dynamics, the persistent correlations of the system dynamics apparently lead to a ballistic behavior for the relatively small numerically accessible numbers of contacts. The behavior of the variance for large numbers of contact as well as for more complex systems undergoing unitary dynamics poses an interesting problem and might provide a novel way to characterize so-called quantum chaotic systems. Presently, the investigation of this problem is hampered by numerical problems because it requires both large-system Hilbert spaces as well as a large number of contacts. Both demands request huge storage and computational capacities, which can possibly be realized with future quantum computers.

We would like to emphasize that the proposed strategy to reduce the backaction by repeated contacts differs from weak measurements specifying the probabilities of so-called quantum trajectories of a continuously measured observable [4–6,34], in several respects: Instead of a continuum of necessarily weak *measurements* determining a quantum trajectory, i.e., with a measurement strength typically scaling with a vanishing time step τ as $\tau^{1/2}$, we consider a discrete sequence of *contacts* which are not restricted to be weak. The final measurement then yields a random number representative for the sum of the sequence of the observable taken at the contacts provided that the contact strength is sufficiently strong such that the spectrum of the considered observable can be resolved with a single measurement of the same strength.

We are aware of the fact that the experimental realization of a continuous pointer which is idle if not in contact with the system might be difficult. We intentionally presented the approach of repeated contacts with an idealized model in order to highlight the principle idea without technical complications being specific for a particular realistic application. The inclusion of a realistic pointer dynamics as well as the consideration of protocols prescribing contacts with variable time delay are doable.

As a particular problem that can be attacked by the presented strategy, we finally mention the diagnosis of a quantum engine performing in finite time. The so-far employed analysis in terms of projective energy measurements [19] suppresses any coherences extending over a single cycle. Their possible impact on the performance with respect to power, efficiency, and reliability is of major importance [35].

ACKNOWLEDGMENTS

This research was supported by the Institute for Basic Science in Korea (Grant No. IBS-R024-Y2).

[1] E. C. G. Sudarshan and B. Misra, J. Math. Phys. **18**, 855 (1977).
[2] J. Yi, P. Talkner, and G.-L. Ingold, Phys. Rev. A **84**, 032121 (2011).
[3] L. Magazzu, P. Talkner, and P. Hänggi, New J. Phys. **20**, 033001 (2018).
[4] M. J. Gagen, H. M. Wiseman, and G. J. Milburn, Phys. Rev. A **48**, 132 (1993).
[5] H. W. Wiseman and G. Milburn, *Quantum Measurement and Control* (Cambridge University Press, Cambridge, 2009).
[6] K. Jacobs and D. A. Steck, Contemp. Phys. **47**, 279 (2006).
[7] J. von Neumann, *Mathematische Grundlagen der Quantenmechanik* (Springer, Berlin, 1932); Engl. trans.: *Mathematical Foundations of Quantum Mechanics* (Princeton University Press, Princeton, NJ, 1955).
[8] D. Bohm, *Quantum Theory* (Prentice Hall, NJ, 1951).
[9] G. Waldherr, A. C. Dada, P. Neumann, F. Jelezko, E. Andersson, and J. Wrachtrup, Phys. Rev. Lett. **109**, 180501 (2012).
[10] F. E. Becerra, J. Fan, and A. Migdall, Nat. Commun. **4**, 2028 (2013).
[11] A. J. Roncaglia, F. Cerisola, and J. P. Paz, Phys. Rev. Lett. **113**, 250601 (2014).
[12] G. de Chiara, A. J. Roncaglia, and J. P. Paz, New J. Phys. **17**, 035004 (2015).
[13] P. Talkner and P. Hänggi, Phys. Rev. E **93**, 022131 (2016).

[14] P. Talkner, E. Lutz, and P. Hänggi, Phys. Rev. E **75**, 050102(R) (2007).
[15] S. E. Venegas-Andraca, Quantum Inf. Proc. **11**, 1015 (2012).
[16] C. M. Bender, D. C. Brody, and B. K. Meister, J. Math Phys. A **33**, 4427 (2000).
[17] R. Kosloff and A. Levy, Ann. Rev. Phys. Chem. **65**, 365 (2014).
[18] Y. Zheng, P. Hänggi, and D. Poletti, Phys. Rev. E **94**, 012137 (2016).
[19] X. H. Ding, J. Yi, Y. W. Kim, and P. Talkner, Phys. Rev. E **98**, 042122 (2018).
[20] N. Van Horne, D. Yum, T. Dutta, P. Hänggi, J. B. Gong, D. Poletti, and M. Mukherjee, npj Quantum Inf. **6**, 37 (2020).
[21] An operation is a linear, completely positive map on the trace-class operators of a Hilbert space [22,23].
[22] K. Kraus, *States, Effects and Operations -Fundamental Notions of Quantum Theory* (Springer-Verlag, Berlin, 1983).
[23] M. Hayashi, *Quantum Information Theory: Mathematical Foundation*, 2nd ed. (Springer, Berlin, 2017).
[24] D. R. Cox and H. D. Miller, *The Theory of Stochastic Processes* (Chapman and Hall, Boca Raton, FL, 1965).
[25] W. Feller, *An Introduction to Probability Theory and its Applications*, 3rd ed., Vol. 1 (Wiley, New York, 1968).
[26] G. Lindblad, Commun. Math. Phys. **48**, 119 (1976).
[27] R. Alicki and K. Lendi, *Quantum Dynamical Semigroups and Applications*, Lect. Notes Phys., Vol. 717 (Springer, Berlin, 1987).
[28] P. Talkner, Ann. Phys. **167**, 390 (1986).
[29] W. Weidlich and H. Haake, Z. Phys. B **186**, 203 (1965).
[30] F. Haake, *Quantum Signatures of Chaos* (Springer-Verlag, Berlin, 2001).
[31] P. Kurzyński and A. Wójcik, Phys. Rev. Lett. **110**, 200404 (2013).
[32] Y. Y. Zhao, N. K. Yu, P. Kurzyński, G. Y. Xiang, C. F. Li, and G. C. Guo, Phys. Rev. A **91**, 042101 (2015).
[33] Z. Bian, J. Li, H. Qin, X. Zhan, R. Zhang, B. C. Sanders, and P. Xue, Phys. Rev. Lett. **114**, 203602 (2015).
[34] D. Yang, A. Grankin, L. M. Sieberer, D. V. Vasilyev, and P. Zoller, Nat. Commun. **11**, 775 (2020).
[35] A. Streltsov, G. Adesso, and M. B. Plenio, Rev. Mod. Phys. **89**, 041003 (2017).